METALS
AND SUPERCONDUCTORS

Temperature Behavior of Electron Transport in Normal-Metal–HTSC Heterojunctions

F. V. Komissinskiĭ[1, 2], G. A. Ovsyannikov[1], and Z. G. Ivanov[2]

[1]*Institute of Radio Engineering and Electronics, Russian Academy of Sciences, Mokhovaya ul. 11, Moscow, 103907 Russia*
e-mail: gena@hitech.cplire.ru
[2]*Chalmers Institute of Technology, S-41296 Göteborg, Sweden*
Received July 25, 2000; in final form, October 6, 2000

Abstract—Current transport in micron-sized normal-metal–high-temperature superconductor heterojunctions ($Au/YBa_2Cu_3O_{6+x}$) was studied for two crystallographic orientations of YBCO films. It is shown that depending on the transport-current flow direction relative to the crystallographic axes of the YBCO film, the electronic transport properties of Au/YBCO heterojunctions with highly transparent boundaries change from quasi-tunneling (along the YBCO c axis) to close-to-Ohmic (in the directions lying in the YBCO basal plane). © 2001 MAIK "Nauka/Interperiodica".

INTRODUCTION

The electronic parameters of high-temperature superconducting (HTSC) metal–oxide materials are very sensitive to oxygen content. $YBa_2Cu_3O_{6+x}$ (YBCO), a typical representative of the HTSCs, is an insulator for oxygen contents of $0 < x < 0.4$ and a superconductor exhibiting metallic conduction along the basal planes at oxygen doping levels of $0.4 < x < 1$ (see, e.g., [1]). An HTSC layer close to an interface with a vacuum or other material can change its parameters from those of a metal to those of an insulator, depending on the extent of external influence on the oxygen content (heating, precipitation of carbon dioxide from the atmosphere, etc.). Another essential feature of the HTSCs is the high anisotropy of their electron transport characteristics [2]. The conductivities for currents flowing along the c axis of YBCO and the directions lying in the (a–b) YBCO basal plane differ greatly. As a result, when the transport current changes its orientation with respect to the crystallographic axes of a superconductor, the ratios of the characteristic resistances of the normal-metal–HTSC (N–S_d) interface, $r = R_N S$ (R_N is the resistance of a junction of area S), which characterize the boundary transparency, can change a hundredfold [3, 4]. Depending on the actual YBCO film orientation and the technology of preparation, N–S_d heterojunctions experimentally exhibit a large variety of properties, from quasi-tunneling [5, 6] to Ohmic characteristics [7]. Heterojunctions with a low boundary transparency ($r > 10^{-4}\ \Omega\ cm^2$) usually have quasi-tunneling characteristics, namely, tunneling at low voltages and an increase in resistance with decreasing temperature [6]. This experimental observation suggests that the surface HTSC layer was depleted in oxygen to the extent that it became an insulator. The quasi-tunneling characteristics of the heterojunctions were not questioned in these conditions. However, in order for the surface layer to be an insulator while the remaining part of the HTSC film is doped by oxygen to the extent corresponding to the superconducting state, one has to admit substantial oxygen content gradients across the film thickness. This condition can hardly be realized in an experiment even when oxygen diffusion along the c axis is weak. The I–V characteristics of N–S_d junctions with a low-transparency boundary in both c and a–b oriented HTSC films frequently exhibited conductivity anomalies even at low voltages, namely, a conductivity peak at zero bias. The reasons for this anomaly were attributed either to the presence of ferromagnetic impurities in the HTSC surface layer [8, 9] or to the formation of bound states as a result of the Andreev reflection at the interface between a d-type superconductor and an insulator [10–12].[1]

In this work, the experimental data obtained on the temperature dependence of the resistance of N–S_d heterostructures and the shape of the I–V curves suggest a conclusion on the mechanism of conduction in normal-metal–HTSC heterojunctions for current flow both along the c axis and along the directions lying in the basal plane of a YBCO.

1. YBCO FILMS AND EXPERIMENTAL SAMPLES

The sequence of the technological operations used to fabricate Au/YBCO heterojunctions is presented in Fig. 1 [13, 14]. Epitaxial YBCO films 150 nm thick were grown by laser ablation at temperatures of 780–800°C and at an oxygen pressure of 0.8 mbar. Epitaxial c-oriented YBCO films were grown on $(001)LaAlO_3$

---

[1] The anomalies in the I–V curves appearing at low bias across our junctions will be discussed in a forthcoming paper.
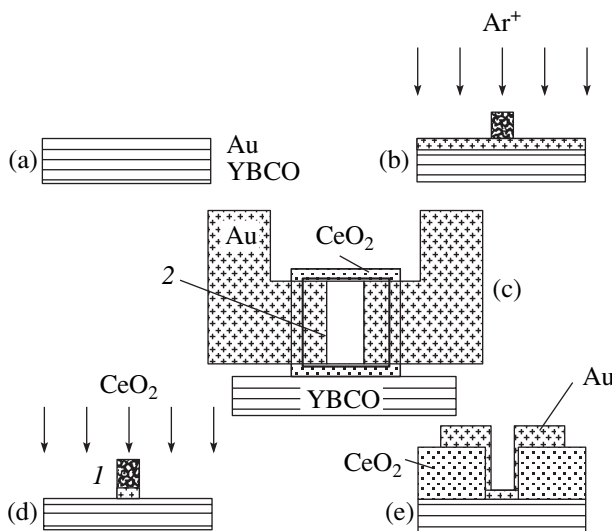
Fig. 1. Sequence of Au/YBCO junction fabrication steps: (a) Deposition of the Au(20 nm)/YBCO(150 nm) double-layer structure; (b) formation of the junction region by photolithography and ion milling; (c) junction geometry (top view); (d) deposition of the 150-nm thick CeO_2 insulating layer; and (e) formation of Au contact pads. (*1*) Photoresistor and (*2*) contact region.

and (110)NdGaO$_3$ (NGO) substrates. Heterostructures fabricated on these substrates provide information on the transport current flowing along the [001]YBCO direction; we shall subsequently call such structures direct heterojunctions (DH). In the work, we also used tilted heterojunctions (TH) in which the [001]YBCO crystallographic axis deviates from the normal to the substrate plane. These films were grown epitaxially on (120)NGO substrates. After YBCO film deposition, a thin layer of normal metal (Au) 20 nm thick was deposited on it without impairing the vacuum (Fig. 1a). The Au layer thickness was increased to 100 nm by additional *ex situ* electron beam deposition (entailing vacuum deterioration). A heterojunction of area $S = 10 \times 10$ μm was produced by photolithography and ion beam milling in an Ar atmosphere (Fig. 1b). To avoid undesirable contact with the YBCO face end, the heterojunction regions were isolated by an amorphous CeO_2 film deposited by laser ablation at 60°C in an oxygen environment at a pressure of 0.2 mbar (Fig. 1d). The isolating layer in the region of the heterojunctions and of the contact pads was removed by explosive photolithography (Fig. 1e). The spatially separated supply of the current and voltage provided in the Au/YBCO heterojunction geometry (Fig. 1c) permits one to measure the heterojunction characteristics by the four-probe technique for $T < T_c$ of the YBCO.

We measured curves *I–V* and the dependences of the resistance *R* on temperature *T* (4.2–300 K) with bias currents in the range 1–5 μA for Au/YBCO heterojunctions and test bridges 4 μm wide located on the same substrate. The critical temperature and width of the

superconducting transition in the YBCO films (T_c and ΔT_c, respectively) were found from the temperature dependence of the magnetic susceptibility for the Au/YBCO heterostructure before junction topology formation. For the *c*-oriented YBCO films, we have $T_c > 88$ K and $\Delta T_c = 0.5$ K. The YBCO films grown on (120)NGO had slightly worse superconducting parameters ($T_c > 85$ K and $\Delta T_c \le 2$ K) because of a lower oxygen content. A decrease in T_c and ΔT_c is typical of films with the *c* axis off the surface normal [14, 15].

X-ray diffraction measurements (θ–2θ scanning) showed that the epitaxial relation (001)YBCO//{110}NGO is retained for both the (110)NGO and (120)NGO substrates; in other words, the [001] direction of the YBCO film is always parallel to the ⟨110⟩NGO directions (if there are more than one of them). The (120)NGO substrates have two directions, [110] and [1$\bar{1}$0]NGO; therefore, two domains, (101) and (109)YBCO, form in the growth, whose *c* axes make angles $\psi = 71.6°$ and $18.4°$ with the surface normal, respectively. Our estimates showed that both domains are present in the YBCO films on the [120]NGO substrates in equal amounts. For both domains, the condition (001)YBCO//{110}NGO holds and one of the basal plane axes (either [100]YBCO or [010]YBCO) lies in the substrate plane. The current in a TH flows primarily along the basal YBCO planes. The contribution of the *c*-axis current in this case is small because of the high YBCO resistivity in this direction. By contrast, in a DH, the transport current flows along the YBCO *c* axis because of the small area of the junction along the *a–b* planes. The parameters of the experimental samples studied are given in the table. Note that at the values $r = 10^{-5}–10^{-7}$ Ω cm^2 observed in the experiment, the characteristic current spreadout length $L_\perp = \sqrt{d_{Au}r/\rho_{Au}}$ ($d_{Au} = 100$ nm and $\rho_{Au} = 10^{-6}$ Ω cm are the thickness and electrical resistivity of the gold film, respectively) [16] significantly exceeds the heterojunction dimensions. Hence, the current spreadout process should not affect the electrophysical parameters of the heterojunctions.
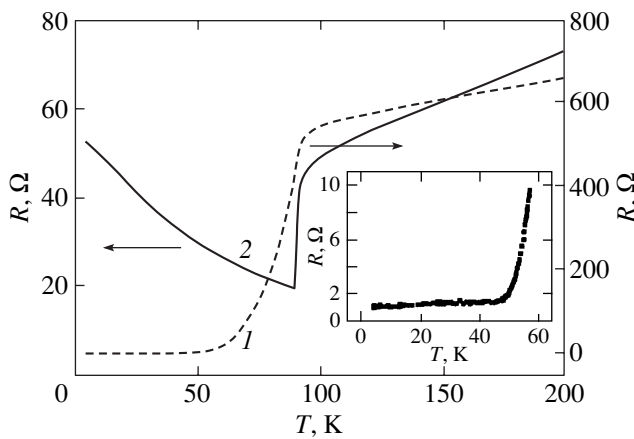
2. EXPERIMENTAL RESULTS

Figure 2 displays *R(T)* plots measured by the three-point technique (with the current and voltage applied to one point on the YBCO electrode) for two types of Au/YBCO heterojunctions. For $T > T_c$, the *R(T)* relations of DHs exhibit metallic conduction, i.e., a decrease in the resistance with temperature, which is characteristic of a transport current flowing in the basal plane of an YBCO film. This is due to the predominant contribution to the measured *R(T)* relation of the conducting HTSC electrode films, which carry current in the YBCO *a–b* planes. At the same time, when the master transport current propagates along the [$\bar{2}$10]NGO direction in a TH, one observes an increase of *R* typical

Low–temperature heterojunction parameters

Sample	T_c, K	$R_N(T = T_c, V = 0)$, Ω	$R_d(0)$, Ω	$R_d(0)/R_N$	$R_N S$, $\mu\Omega$ cm^2
DH					
P32J2	89.3	33.2	103.0	3.1	33.2
P32J3	89.5	19.5	52.0	2.7	19.5
P32J4	89.9	22.9	55.3	2.4	22.9
P34J3	89.2	56.1	102.0	2.1	56.1
TH					
H2J2	18.7	1.6	0.7	0.4	1.6
H2J3	48.2	1.6	1.0	0.6	1.6
H2J4	40.1	1.8	1.3	0.7	1.8
H5J2	42.3	0.4	0.2	0.5	0.4
H5J3	60.3	0.3	0.2	0.7	0.3
H5J4	61.1	0.5	0.3	0.6	0.5

of transport along the c axis of the YBCO. The temperatures T_c of the microbridges in the THs studied turn out to be lower than those of the YBCO films immediately after Au/YBCO heterostructure deposition, which is apparently due to oxygen escaping from the surface layer of the YBCO films in the course of ion milling. In the THs, oxygen diffuses out of the basal planes of the YBCO films on the surface much more intensively than in the DHs. As a result, the T_c of the bridges on the (120)NGO substrates is lower than that of the original Au/YBCO heterostructures by 5–10 K.
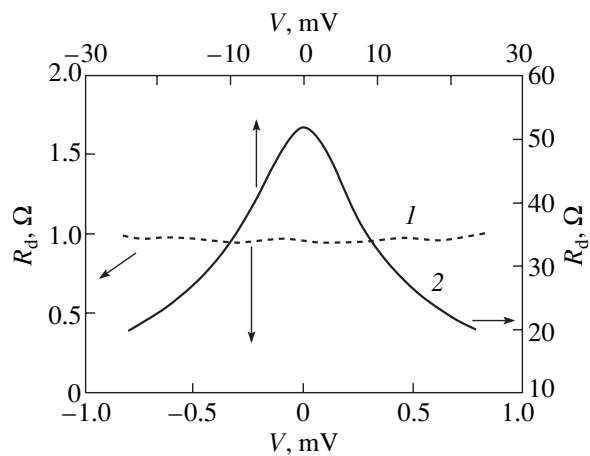
The $R(T)$ relations change dramatically for $T < T_c$; more specifically, in the DHs, one observes a growth characteristic of the superconductor–insulator–normal-metal tunneling junctions (SIN, with I standing for the insulator), while in the THs, the resistance falls off monotonically with decreasing temperature.
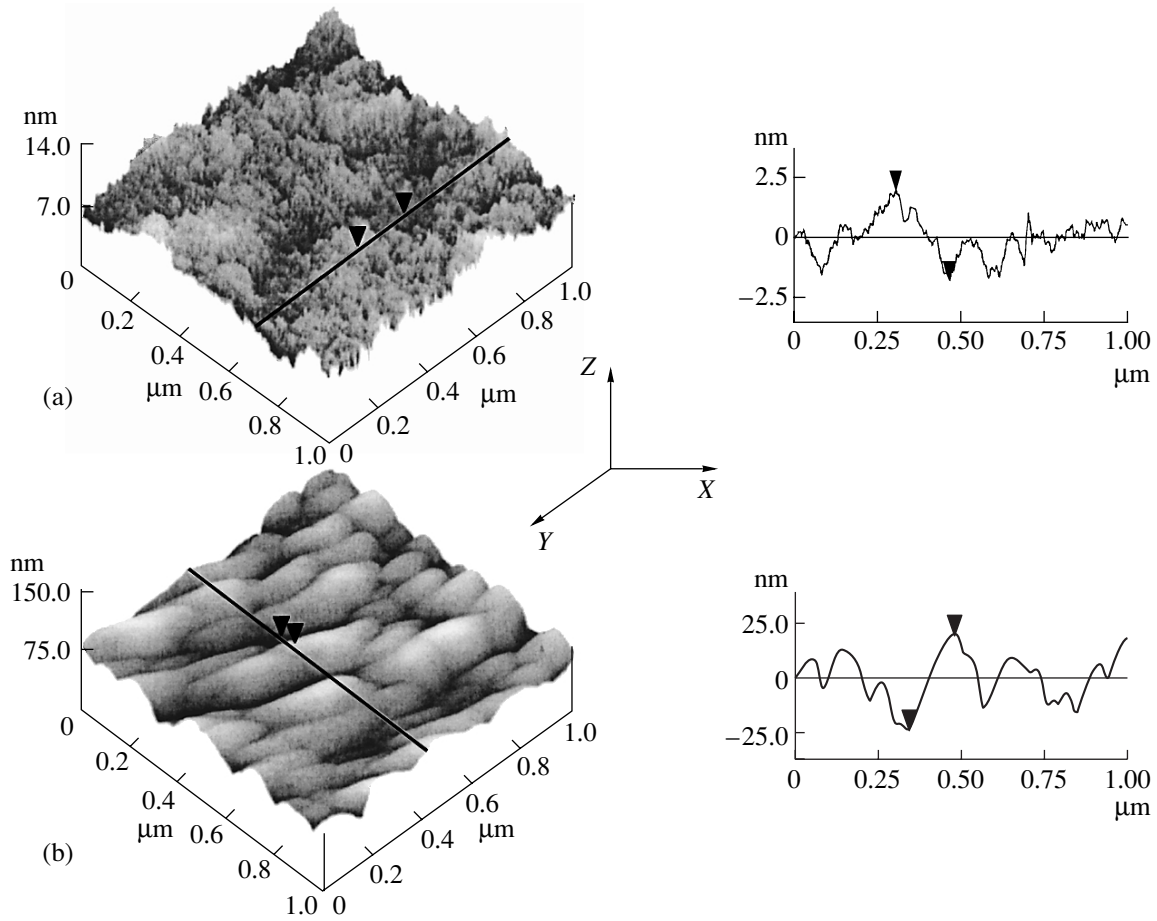
Figure 3 presents the dependences of the differential resistance of the Au/YBCO heterojunctions on the bias $R_d(V)$. One likewise observes substantial differences both in the characteristic interface resistance r and in the field dependence. For the THs, $r_{ab} = 10^{-7}$–10^{-6} Ω cm^2, whereas r_c for the DHs is larger by one to two orders of magnitude (see the table).

To estimate the interface surface, we studied the YBCO film surface morphology with atomic force microscopy. As shown by YBCO film profile measurements, the maximum surface roughness of the (001)YBCO films over an area of 1×1 μm is $\delta_c \approx 4$ nm (in Fig. 4a, rms = 2 nm). The roughness of tilted YBCO films on (120)NGO is substantially larger: $\delta_{ab} \approx 45$ nm (Fig. 4b), with rms = 50 nm.

Fig. 2. $R(T)$ dependences for (*1*) TH H2J3 and (*2*) DH P32J3. Inset shows the low-temperature part of the $R(T)$ plot for the TH H2J3.

Fig. 3. $R_d(V)$ relations for (*1*) TH H2J3 and (*2*) DH P32J3 measured at $T = 4.2$ K.

Fig. 4. YBCO film surface profile measurements with an atomic force microscope. (a) DH, the vertical and horizontal mark separations are 3.7 and 160 nm, respectively; (b) TH, the vertical and horizontal mark separations are 44 and 132 nm, respectively.

3. DISCUSSION OF EXPERIMENTAL RESULTS

It is well known that the resistance of metals connected in series, even if they are in direct contact, is not the sum of their resistances if the Fermi momenta of the contacting materials are different [4, 17, 18]. As a result of the mismatch between the electronic parameters of two contacting materials, in particular, of the Fermi momenta p_{fi} ($i = 1, 2$), the characteristic contact resistance becomes [17]

$$r_c^{-1} = (e^2 p_f^2 / 2\pi^2 \hbar^3) 2 \langle xD(x) \rangle, \tag{1}$$

where $p_f = \min\{p_{f1}, p_{f2}\}$, $D(x)$ is the boundary transparency, and the angular brackets denote averaging over the directions of the quasiparticle momenta. In the case of a sharp and plane interface between two metals with $p_{f1} \ll p_{f2}$ and of spherical Fermi surfaces, the transparency is given by [17]

$$D(x) = 4x p_{f1} / p_{f2}, \quad 2 \langle xD(x) \rangle = 8 v_{f1} / 3 v_{f2}, \tag{2}$$

where v_{fi} ($i = 1, 2$) are the Fermi velocities in the contacting materials. One readily sees that in the case of a large enough Fermi velocity mismatch between the

contacting metals, the transparency $D \ll 1$ even in the absence of an insulating spacer. If, however, the interface is smooth on a scale of $\hbar/p_f$, then $D \approx 1$, irrespective of the Fermi momentum difference between the materials in contact [17].

Using for the estimation of p_f the relation [19]

$$p_f^2 = 3\pi^2 \hbar^3 / (e^2 \rho l) \tag{3}$$

and the resistivities of the YBCO film of sample H5 ($\rho_c = 2 \times 10^{-1}$ Ω cm along the c axis and $\rho_{ab} = 4 \times 10^{-3}$ Ω cm in the basal plane, as determined from bridge measurements), as well as the mean free path lengths $l_c = 1$ nm [20] and $l_{ab} = 10$ nm [21] ($\rho_c l_c = 2 \times 10^{-8}$ and $\rho_{ab} l_{ab} = 4 \times 10^{-9}$ Ω cm^2), we obtain $p_{fab}/p_{fc} \approx 2.2$ for the Fermi momentum anisotropy. As shown by our estimates, this value of the ratio p_{fab}/p_{fc} still permits one to use relations (1)–(3) to calculate the transport along the c axis. Using the experimental values for r and ρl from Eqs. (1) and (3), we obtain $2\langle xD(x) \rangle \approx 7 \times 10^{-4}$ for the interface transparency of sample P32J3, which is close to the value $2\langle xD(x) \rangle \approx 8 \times 10^{-4}$ calcu-

lated from Eq. (2) under the assumption of the carrier effective mass along the c axis being $m = 100 \, m_e$ [22]. The difference between the transparencies obtained by different techniques is most likely associated with the fact that the ρ_c of YBCO films derived from bridge resistance measurements is smaller by an order of magnitude than those for the thin layer at the $N–S_d$ interface, which were determined from four-point measurements of the junction resistance at $T = T_c$.

When determining the experimental value of the transparency along the a–b plane in THs, one should take into account the layered HTSC structure. As a result, in averaging over the momentum directions, the main contribution should be due to electrons within the angular range $\alpha < \arctan(d/\lambda_N) \approx 84°$ ($\lambda_N \approx 0.12$ nm is the de Broglie wavelength for electrons in Au, and $d \approx 1.2$ nm is the distance between the CuO planes in YBCO). One should also take into account the sharpness of the interface, which radically changes its transparency. A comparison of δ_{ab} and δ_c (Fig. 4) with λ_{ab} and λ_c (the de Broglie wavelength for electrons in YBCO), respectively, shows that in the THs ($\delta_{ab} \gg \lambda_{ab} \approx 2$ nm), the interface is smooth, whereas in the DHs with $\delta_c \sim \lambda_c \approx 4$ nm, we most likely have a sharp interface. As a result, relation (2) is applicable to the DHs, while the interface transparency in the THs is substantially larger ($D_{ab} \approx 1$); however, when averaged over the momentum directions, we obtain for the THs

$$2\langle xD(x)\rangle = (\lambda_N/d)^2 = 10^{-2}. \qquad (4)$$

Note that the value $2\langle xD(x)\rangle = 9 \times 10^{-3}$, found from Eqs. (1) and (3), is close to the estimate in Eq. (4) made for the H5J3 sample. Hence, while the transparency of a smooth interface for electrons with momenta oriented close to the normal is of order unity, the transparency averaged over the momentum directions is small because of the layered structure of the YBCO and does not contribute noticeably to the characteristic resistance of the interface. Relation (4) also shows that for abrupt $N–S_d$ interfaces, r_{ab} is nearly equal to r_c, despite the large anisotropy of the Fermi momenta.

As shown by calculations [4, 17], for $v_{f1}/v_{f2} \ll 1$, the $N–S_d$ and NIS junctions have similar electrophysical properties. Figure 3 shows that the I–V curves obtained in our experiment for $T \ll T_c$ are, on the whole, close to those measured on NIS junctions; namely, one observes an increase of R_d at low bias. However, in our experiment, in contrast to the theory of [17], R_d does not exhibit any features associated with the YBCO superconducting gap. One could conceive of two reasons for the diffuse character of the gap feature in the I–V curves. The first of them is the existence of a direct contact between the superconductor and the normal metal. By [17], for $T = 0$, we have $R_d(\Delta/e)/R_N = \langle xD(x)\rangle$; i.e., the I–V characteristics of NcS junctions ("c" stands for constriction) do not have a divergence of

the $((eV)^2 - \Delta^2)^{-1/2}$ type characteristic of NIS junctions for $T \ll T_c$. Second, the absence of a gap feature in the I–V curves agrees with the model of a superconductor with gapless superconductivity, including a d-type superconducting order parameter [11, 12]. By calculations [11], the feature in the I–V characteristics at $eV \approx \Delta$ caused by growth of the density of states of a d superconductor at energies $\varepsilon \approx \Delta$ yields a logarithmic dependence $R_d \sim \ln(T)$ and $\ln(\||eV| - \Delta|)$, which is subject to a temperature-induced spread, as in the case of gapless superconductivity. Note that the Nb–Au–YBCO heterojunctions, as well as the Pb–Au–YBCO structures produced on c-oriented YBCO films, exhibit a gap feature of a low-temperature superconductor, but the YBCO I–V curves do not have a gap feature at $V \approx \Delta/e$ [23, 24]. This is an additional indication of the YBCO order parameter exerting a fairly strong effect on gap feature formation in the I–V curves at $V \approx \Delta/e$. While both these effects cause a smoothing of the gap feature at $V \approx \Delta/e$, the tunnel feature at $V \ll \Delta/e$ observed experimentally persists up to fairly high interface transparencies ($D \sim 10^{-1}$).

The number of quasiparticles excited at low temperatures ($kT \ll \Delta$) in a superconductor with s-type order parameter symmetry decreases exponentially with temperature; hence, the magnitude of $R_d(0) \sim \exp(-\Delta/T)$ in SIN junctions increases proportionally. The presence of zero order parameter sites in a superconductor with d-type pairing makes it possible to excite quasiparticles even at a very low temperature, $T \ll \Delta$. As a result, $R_d(0)$ should grow more slowly with decreasing T than occurs in s superconductor junctions [11]. The existence of direct conduction in a junction acts in the same sense. In addition to the scattering mechanism originating from a p_{fi} mismatch, one observes Andreev reflection for electrons with energies $\varepsilon < p_f^2/2m$. The electrons carrying the current in the normal metal are reflected from the interface with a superconductor in the form of a hole with about the same $|p_f|$, and the current in the superconductor is transported by superconducting pairs [17]. As a result of the combined action of the two above mechanisms, the temperature dependence of $R_d(0)$ differs from the exponential $\exp(-\Delta/kT)$. As seen from Fig. 5, the conductivity $\sigma = 1/R_d(0)$ for a DH does decrease in our experiment by a power law with temperature.

An additional experiment indicating the Fermi momentum mismatch as a factor governing the electrophysical parameters of the heterostructures studied is annealing in an oxygen atmosphere. It was experimentally established earlier that the main process taking place in heterostructures made of HTSCs with noble metals (silver, gold, platinum, etc.) and subjected to annealing is an increase in the oxygen content in the surface layer of the (001)YBCO film [25, 26]. When heated in an oxygen environment, an increase in oxygen content in the YBCO surface layer is accompanied
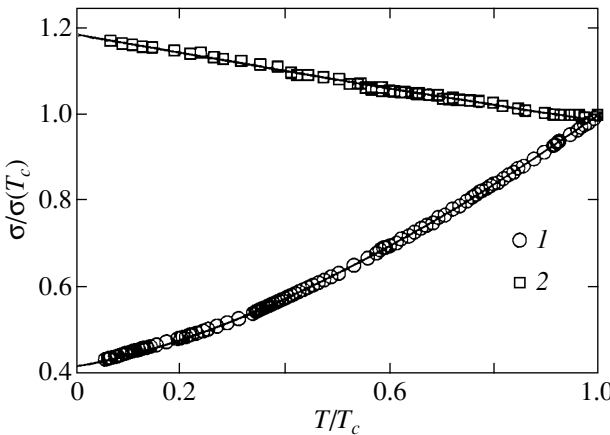
Fig. 5. Normalized temperature dependences of the conductivity: (*1*) for the DH and (*2*) for the TH measured for $T < T_c$. The corresponding fitting curves are shown by solid lines: $\sigma/\sigma(T_c) \approx 0.4 + 0.3(T/T_c) + 0.3(T/T_c)^2$ for a DH, and $\sigma/\sigma(T_c) \approx 1.2 - 0.2(T/T_c)$ for a TH.
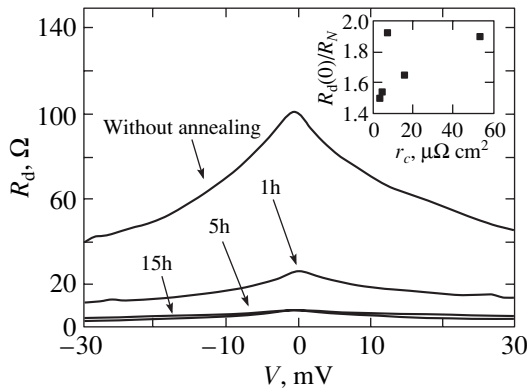
Fig. 6. Variation of the $R_d(V)$ dependence for the P34J3 DH with annealing in an atomic-oxygen environment at $T = 600°C$. Inset shows the $R_d(0)/R_N$ dependence on r_c, which characterizes the variation of DH conductivity in the course of the anneal.

by a change in its $\rho_c l_c$ and, as a consequence, the Fermi momentum of YBCO increases and r_c decreases. Unlike other noble metals, gold is not observed to diffuse in YBCO. Figure 6 displays $R_d(V)$ relations for a DH obtained after the anneal of a sample for 0, 1, 5, and 15 h in an oxygen environment at $T = 600°C$. The value of r_c decreases rapidly with increasing anneal time to reach $r_c = 4 \times 10^{-6}\ \Omega\ cm^2$ after 5-h of annealing in place of the original $r = 5.6 \times 10^{-5}\ \Omega\ cm^2$. Further annealing for 15 h did not noticeably affect the value of r. Because the I–V curve in our experiment does not undergo a qualitative change in shape, the surface layer S_d is located, most probably, on the metallic (superconducting) side of the transition and saturation with oxygen

changes its conduction parameters, in particular, the Fermi momentum. As a result, as the oxygen content increases, the resistance of the interface r, which is determined by its transparency D and the value of p_f, should change; this is exactly what was observed in the experiment. The quasi-tunneling component, which can be characterized by the ratio $R_d(0)/R_N$, decreases with annealing, which causes a decrease in r_c (see inset to Fig. 6). One readily sees that by the end of the anneal, the $R_d(0)/R_N$ ratio decreased from 2 to 1.5, while r_c changed by an order of magnitude. This behavior of the I–V curves of heterojunctions is in qualitative agreement with the calculations of [17]; namely, as the Fermi momentum mismatch decreases, the quasi-tunneling I–V characteristic transfers to the I–V curve of junctions with an ScN-type direct conduction. For $D \approx 1$, the properties of the junctions are described by the model of the ScN junction, for which $R_d(0)/R_N = 0.5$ [17].

In a TH, as seen from Figs. 2–4, $R_d(V) \approx$ const within the bias range considered and $R(T)$ falls off linearly with temperature. All this is typical of an $N–S_d$ junction with direct (not tunneling) conduction. Note that r is changed in a TH by an order of magnitude compared with that of a DH and that the transparencies differ by three orders of magnitude because of the additional effect of the roughness of the interface separating the two materials.

Thus, we have observed in *c*-oriented and tilted Au/YBCO heterostructures a strong anisotropy in the temperature dependence of the resistance and the I–V curves, which are caused by a change in the direction of the transport current flowing through the normal-metal–YBCO interface. It has been shown that the experimental results obtained can be described within the model of direct contact between the normal metal and the HTSC, if the substantial mismatch in the Fermi momenta p_{fi} between the materials in contact is taken into account. For a large p_{fi} mismatch, a situation met usually in heterostructures grown on *c*-oriented YBCO films, one observes quasi-tunneling characteristics and the heterostructures on YBCO films with a tilted *c* axis are close in properties to Ohmic contacts because of the smaller p_{fi} mismatch and the interface roughness, which reduces electron reflection from the interface. The oxygen-depleted layer existing on the (001)YBCO surface increases the characteristic heterostructure resistance; however, in our experiments, the doping level of this layer is such that it is always on the metallic side of the metal–insulator transition.

ACKNOWLEDGMENTS

REFERENCES

1. *The Gap Symmetry and Fluctuations in High-T_c Superconductors*, Ed. by J. Bok, G. Deutscher, D. Pavuna, and S. A. Wolf (Plenum, New York, 1998), NATO ASI Ser., Ser. B **371**, 560 (1998).

2. S. W. Tozer, A. W. Kleinsasser, T. Penney, *et al.*, Phys. Rev. Lett. **59** (15), 1768 (1987).

3. R. Krupke and G. Deutscher, Phys. Rev. Lett. **83**, 4634 (1999).

4. M. Yu. Kupriyanov and K. K. Likharev, IEEE Trans. Magn. **27** (2), 2460 (1991).

5. S. C. Sanders, S. E. Russek, C. C. Clickner, and J. W. Ekin, Appl. Phys. Lett. **65** (17), 2232 (1994).

6. S. G. Lee, Y. Huh, Y. S. Hwang, *et al.*, Physica C (Amsterdam) **282–287**, 1491 (1997).

7. Yuzi Xu, J. W. Ekin, S. E. Russek, *et al.*, IEEE Trans. Appl. Supercond. **7** (2), 2836 (1997).

8. M. Gurvitch, J. M. Valles, Jr., A. M. Cucolo, *et al.*, Phys. Rev. Lett. **63** (9), 1008 (1989).

9. J. Lesueur, L. H. Greene, W. L. Feldmann, and A. Inam, Physica C (Amsterdam) **191**, 325 (1992).

10. Chia-Ren Hu, Phys. Rev. Lett. **72** (10), 1526 (1994).

11. Yu. S. Barash, A. V. Galaktionov, and A. D. Zaikin, Phys. Rev. B **52** (1), 665 (1995).

12. Y. Tanaka and S. Kashiwaya, Phys. Rev. Lett. **74** (17), 3451 (1995).

13. F. V. Komissinskiĭ, G. A. Ovsyannikov, N. A. Tulina, and V. V. Ryazanov, Zh. Éksp. Teor. Fiz. **116** (6), 2140 (1999) [JETP **89**, 1160 (1999)].

14. F. V. Komissinskiĭ, G. A. Ovsyannikov, N. A. Tulina, and V. V. Ryazanov, in *Proceedings of the XXXI Conference on Physics of Low Temperatures, Moscow, 1998*, p. 236.

15. Y. Y. Divin, U. Poppe, P. M. Shadrin, *et al.*, in *Proceedings of the 2nd European Conference on Applied Superconductivity, EUCAS, Edinburgh, 1995*, Inst. Phys. Conf. Ser. 148, **2**, 1359 (1995).

16. A. M. Klushin, A. Golubov, W. Prusseit, and H. Kolstedt, J. Low Temp. Phys. **106**, 265 (1997).

17. A. V. Zaĭtsev, Zh. Éksp. Teor. Fiz. **86** (5), 1742 (1984) [Sov. Phys. JETP **59**, 1015 (1984)].

18. G. E. Blonder, M. Tinkham, and T. M. Klapwijk, Phys. Rev. B **25** (7), 4515 (1982).

19. P. G. de Gennes, *Superconductivity of Metals and Alloys* (Benjamin, New York, 1966; Mir, Moscow, 1968).

20. J. Yoshida, T. Hashimoto, S. Inoue, *et al.*, Jpn. J. Appl. Phys., Part 1 **31** (6A), 1771 (1992).

21. K. Krishana, J. M. Harris, and N. P. Ong, Phys. Rev. Lett. **75** (19), 3529 (1995).

22. L. N. Bulaevskiĭ, V. L. Ginzburg, and A. A. Sobyanin, Zh. Éksp. Teor. Fiz. **94** (7), 355 (1988) [Sov. Phys. JETP **67**, 1499 (1988)].

23. A. S. Katz, A. G. Sun, R. C. Dynes, and K. Char, Appl. Phys. Lett. **66** (1), 105 (1995).

24. P. V. Komissinski, E. Il'ichev, G. A. Ovsyannikov, *et al.*, cond-mat/0008077.

25. J. W. Ekin, T. M. Larson, N. F. Bergen, *et al.*, Appl. Phys. Lett. **52** (21), 1819 (1988).

26. Siu-Wai Chan, L. Zhao, C. Chen, *et al.*, J. Mater. Res. **10** (10), 2428 (1995).

Translated by G. Skrebtsov